Annu. Rev. Nucl. Part. Sci. 2000. 50:37–69

ENERGY LOSS IN PERTURBATIVE QCD

R. Baier
Fakultät für Physik, Universität Bielefeld, D-33501 Bielefeld, Germany;
e-mail: baier@physik.uni-bielefeld.de

D. Schiff
LPT, Université Paris-Sud, Bâtiment 210, F-91405 Orsay, France;
e-mail: dominique.schiff@th.u-psud.fr

B. G. Zakharov
L. D. Landau Institute for Theoretical Physics, 117334 Moscow, Russia;
e-mail: bgz@landau.ac.ru

Key Words dense nuclear matter, quark-gluon plasma, gluon radiation, relativistic heavy-ion collisions

■ **Abstract** We review the propagation of energetic partons in hot or cold QCD matter, as known from recent work. We summarize advances in the understanding of both collisional and radiative energy loss. Our emphasis is on radiative energy loss, which has very interesting properties that may help to detect the quark-gluon plasma produced in heavy-ion collisions. We describe two different theoretical approaches, which lead to the same radiated gluon energy spectrum. The case of a longitudinally expanding QCD plasma is investigated. The energy lost by a jet with given opening angle is calculated with the aim of making predictions for the suppression (quenching) of hard jet production. Phenomenological implications for the difference between hot and cold matter are discussed. Numerical estimates of the loss suggest that it may be significantly greater in hot matter than in cold. This makes the magnitude of the radiative energy loss a remarkable signal for quark-gluon plasma formation.

CONTENTS

1. INTRODUCTION

Over the past few years, much work has been devoted to the propagation of high-energy partons (jets) through hot and cold QCD matter. The jet $p_\perp$ broadening and the gluon radiation induced by multiple scattering have been studied, as well as the resulting radiative energy loss of the jet. These studies are extensions to QCD of the analogous QED problem considered long ago by Landau et al (1, 2). Recent measurements (3) (reviewed in Reference 4) confirm the theoretical predictions in the QED case to good accuracy.

As in QED, coherent suppression of the radiation spectrum takes place when a parton propagates in a QCD medium. New and interesting predictions are found. When a high-energy parton traverses a length L of hot or cold matter, the induced radiative energy loss is proportional to L^2. The energy loss of a high-energy jet in a hot QCD plasma appears to be much larger than in cold nuclear matter even at moderate temperatures of the plasma, $T \sim 200$ MeV.

Because the order of magnitude of the effect in hot matter is so much greater, energy loss is an observable and remarkable signal of the production of the quark-gluon plasma (QGP). Indeed, there has been a proposal to measure the magnitude of "jet quenching" in the transverse momentum spectrum of hard jets produced in heavy-ion collisions, since jet quenching is the manifestation of energy loss as seen in the suppression and change of shape of the jet spectrum compared with hadron data.

This review[1] is organized as follows. The case of elastic parton scattering giving rise to the collisional energy loss, especially in hot matter, is presented in Section 2. In Section 3, we give the basic elements of the equations and describe the coherent pattern of the gluon radiative spectrum induced by multiple scattering. We derive the induced energy loss and the jet transverse momentum broadening in terms of phenomenologically significant quantities. Section 4 is devoted to the path integral approach, which provides another derivation of the induced radiative spectrum. For heavy-ion collisions, the case of an expanding QCD plasma is more realistic, and therefore Section 5 deals with the corresponding energy loss calculation. In Section 6, we investigate the angular dependence of the radiative gluon spectrum. The dependence of the energy loss on the jet cone size is analyzed. Section 7 is devoted

[1]We concentrate on the more recent theoretical advances. References to earlier work are found in the cited papers.

to estimates of the energy loss in hot QCD matter and in nuclear matter, and orders of magnitude are given. An interesting finding is that the energy loss in the case of a hot QCD medium is quite collimated. Finally, experimental indications are briefly reviewed, and we close with a look to the future.

2. COLLISIONAL ENERGY LOSS IN QCD

The electromagnetic energy loss of a charged particle in matter is well studied (5, 6). Similar mechanisms are responsible for the energy loss of a fast quark or gluon (jet) propagating through dense QCD matter.

In this section, we discuss the loss caused by elastic collisions of the propagating quark or gluon off the (light) partons that form the dense QGP. We consider in some detail the loss of a test quark Q traversing a plasma, with quarks q and gluons g interacting elastically as $Qq \to Qq$ and $Qg \to Qg$ (7); for a review, see Reference (8).

The energy loss per unit length depends on the density ρ_p of the plasma constituents p (with momentum k) and on the differential cross section weighted by the energy transfer $\omega = E - E'$, where $E(E')$ is the energy of the incoming (scattered) Q,

$$-\frac{dE}{dz} = \sum_{p=q,g} \int d^3k \rho_p(k) \int dq^2 \, J\omega \frac{d\sigma^{Qp\to Qp}}{dq^2}. \qquad 1.$$

J denotes the flux factor and q^2 the invariant (four) momentum transfer. Small values of q^2 dominate the collisions,

$$\frac{d\sigma^{Qp\to Qp}}{dq^2} \simeq C_p \frac{2\pi\alpha_s^2}{(q^2)^2}, \qquad 2.$$

with $C_q = \frac{N_c^2-1}{2N_c^2}$, $C_g = 1$ for N_c colors. For a QGP in thermal and chemical equilibrium, the densities are given for N_f flavors by

$$\rho_q = \frac{4N_cN_f}{(2\pi)^3} n_F(k), \; \rho_g = \frac{2\left(N_c^2-1\right)}{(2\pi)^3} n_B(k), \qquad 3.$$

in terms of the Fermi-Dirac (Bose-Einstein) distributions $n_F(n_B)$. Although the factor ω in Equation 1 improves the Rutherford singularity of Equation 2, a logarithmic dependence still remains after the q^2 integration. This dependence has to be screened by medium effects, i.e. with a cut-off related to the Debye mass (9): $-q_{\min}^2 \simeq m_D^2 = O(\alpha_s T^2)$. Noting that $J\omega \simeq \frac{q^2}{2k}$ (when $E, E' \gg k \simeq O(T)$), one obtains (7, 8)

$$-\frac{dE}{dz} = \pi\alpha_s^2 \sum_p C_p \int \frac{d^3k}{k} \rho_p(k) \ln\frac{q_{\max}^2}{q_{\min}^2} \simeq \frac{4\pi\alpha_s^2T^2}{3}\left(1+\frac{N_f}{6}\right)\ln\frac{cE}{\alpha_sT}, \qquad 4.$$

with c a numerical constant of $O(1)$ and $N_c = 3$. The strong coupling constant may be evaluated at the scale $\alpha_s(T)$ for high temperature T.

It has been pointed out (7) that because of the T^2 dependence of Equation 4, the collisional loss is proportional to $\sqrt{\epsilon}$, i.e. the square root of the QGP energy density, which in leading order in the coupling constant is given by $\epsilon = 8\pi^2 T^4(1 + 21N_f/32)/15$ (for a recent review, see Reference 10).

A proper and consistent treatment of the screening effects of the plasma in the low (soft) exchange momentum region of the collisions is indeed possible in the thermal field–theoretical framework (9), using resummed perturbation theory at high temperature. This method, developed by Braaten & Pisarski (11, 12), allows one to calculate the hard thermal loop (HTL) corrections to the propagator of the exchanged gluon in the $Qq \to Qq$ and the $Qg \to Qg$ processes. The quantum field–theoretical calculation of the energy loss of a quark requires the evaluation of the discontinuity of the self-energy diagrams (see Figure 1).

For the soft momentum exchange [i.e. $q < q_c = O(g^{1/2}T)$], the HTL gluon propagator contributes, whereas for the hard momentum exchange ($q \simeq T$), the tree-level elastic scattering (Figure 1*b*) contributes (13).

The momentum cut-off q_c drops out in the sum of soft and hard contributions. It is important to note that Landau-damping effects, because of the negative q^2 values in Equation 1, screen successfully the low-q^2 region, leading to a well-defined result for dE/dz (at least to leading order in the coupling constant).

As an example, the result is illustrated in Figure 2, where the energy loss of a charm quark is shown by the dashed curve, using parameters characteristic for a thermalized QGP as expected in ultra-relativistic heavy-ion collisions.

For light quarks, the collisional energy loss for a jet propagating in a hot medium of $T = 0.25$ GeV amounts to 0.2–0.3 GeV/fm (8, 14), in agreement with the estimates of Reference (7), as shown in Figure 2 (dotted curve). For a gluon jet, the loss is predicted to be larger by the color factor $2N_c^2/(N_c^2 - 1) = 9/4$ than for the quark jet.

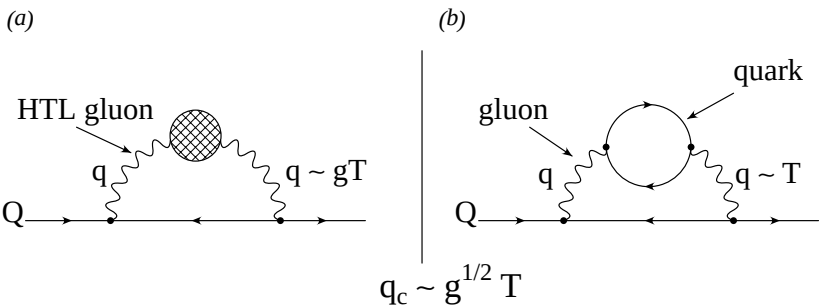

Figure 1 Self-energy diagrams contributing to the collisional energy loss (*a*) in hard thermal loop (HTL) resummed perturbation theory for soft exchanged momentum and (*b*) in leading order for hard exchanged momentum.

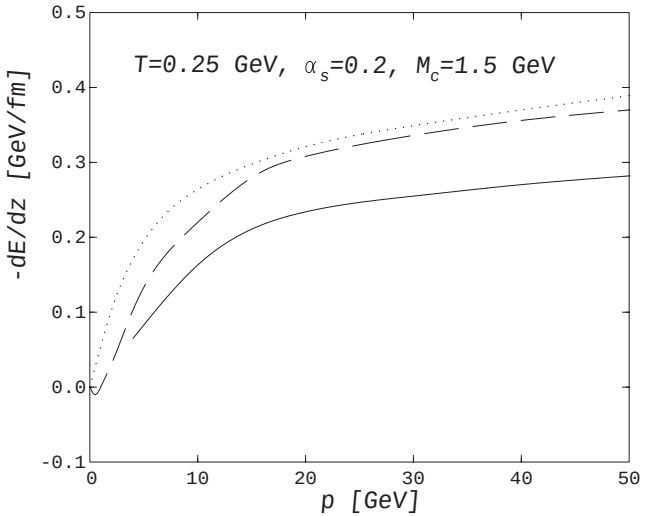

Figure 2 Collisional energy loss of a charm quark as a function of its momentum. The quark propagates through an out-of-chemical-equilibrium plasma with fugacity factors $\lambda_g = 1, \lambda_q = 0$ (solid curve) (16). The dashed curve shows the equilibrium result of Reference (13); the dotted curve shows the original prediction by Bjorken (7).

Since the QGP expected to be produced at the RHIC and LHC colliders is likely to be out of chemical equilibrium, it is necessary to investigate the energy loss in this case (15, 16). Indeed, even away from chemical equilibrium, dynamical screening remains operational within the HTL-resummed perturbation theory. More explicitly, the collisional energy loss for a heavy quark (mass M) that propagates through a QGP parameterized in terms of the distribution functions $\lambda_q n_F$ and $\lambda_g n_B$ becomes (16)

$$-\frac{dE}{dz} = 2\alpha_s \tilde{m}_g^2 \ln\left[0.920\frac{\sqrt{ET}}{\tilde{m}_g}\, 2^{\lambda_q N_f/(12\lambda_g + 2\lambda_q N_f)}\right]. \qquad 5.$$

Here $\lambda_{q,g}$ are the fugacity factors describing chemical nonequilibrium. This expression is valid for energetic quarks with $E \gg M^2/T$ and for $\lambda_q = \lambda_g = 1$ contains the original result of Reference (13). The screening mass parameter is

$$\tilde{m}_g^2 = 4\pi\alpha_s(\lambda_g + \lambda_q N_f/6)T^2/3. \qquad 6.$$

For comparison, the solid curve in Figure 2 shows the loss for the interesting case of the "early plasma phase," which is dominated by gluons ($\lambda_g = 1, \lambda_q = 0$), so that the loss is exclusively due to elastic $Qg \to Qg$ scattering mediated by gluon exchange.

In summary, even when the partons propagating in hot matter have a large momentum, the collisional energy loss per unit length turns out to be less than $O(1)$

GeV/fm when reasonable values for α_s and T are taken. This estimate may be compared with the value for the hadronic string tension, $\kappa \simeq 1$ GeV/fm, which measures the slowing down of a high-momentum quark in (cold) nuclear matter (17).

3. RADIATIVE ENERGY LOSS IN QCD

3.1 Model, Basic Parameters, and Equations

We imagine a very energetic quark of energy E propagating through a QCD medium of finite length L. Multiple scattering of this projectile in the medium induces gluon radiation, which gives rise to the quark energy loss.

The main assumption (18, 19) is that the scattering centers are static and uncorrelated (in the spirit of the Glauber picture). We thus focus on purely radiative processes, since the collisional energy loss vanishes in the case of static centers.

We define a normalized quark-"particle" cross section

$$V(Q^2) = \frac{1}{\pi\sigma}\,\frac{d\sigma}{dQ^2}, \qquad 7.$$

where Q is the two-dimensional transverse momentum transfer normalized by an appropriate scale:

$$\vec{Q} = \frac{\vec{q}}{\mu},$$

and

$$\sigma = \int \frac{d^2\sigma}{d^2Q}\, d\vec{Q}. \qquad 8.$$

In the case of a hot QCD plasma, the "particle" is a quark or gluon, and in the case of cold matter, it is a nucleon. It is usually assumed for diffractive kinematics with very large incident energy that $d^2\sigma/d^2Q$ depends only on $\vec{Q}$. The scale μ characteristic of the medium is conveniently taken as the Debye screening mass in the hot case and as a typical momentum transfer in a quark-nucleon collision. The condition that the independent scattering picture be valid may be expressed as

$$\mu^{-1} \ll \lambda, \qquad 9.$$

where $\lambda = 1/\rho\sigma$ is the parton mean free path in the medium of density ρ. We assume that a large number of scatterings take place, that is

$$L \gg \lambda. \qquad 10.$$

Since successive scatterings are independent, the parton propagation is "time-ordered," and time-ordered perturbation theory is the natural framework in which to calculate the radiation amplitude. Let us sketch the basic equations (see References

20, 21 for further details). We number the scattering centers in sequence of the interaction time and write for the radiation spectrum induced by N scatterings

$$\omega\frac{dI}{d\omega} = \frac{\alpha_s}{2\pi^2}\int d\vec{k}_\perp \left\langle \sum_{i=1}^{N}\sum_{j=1}^{N} \vec{J}^i_{\rm eff}\cdot\vec{J}^{j\dagger}_{\rm eff}\, e^{i(\varphi_i-\varphi_j)}\right\rangle, \qquad 11.$$

where $\vec{J}^i_{\rm eff}$ is an effective current for the gluon emission induced by the center i. It includes color factors consistent with the overall normalization to the elastic scattering cross section. The phase φ_i is associated to time t_i (longitudinal coordinate z_i) by $\varphi_i = t_i k_\perp^2/\omega$.

The brackets indicate averaging—over momentum transfers and over z_i—for which a simplified model is

$$\langle(\cdots)\rangle \Leftrightarrow \int\prod_{\ell=1}^{N-1}\frac{d\Delta_\ell}{\lambda}\exp\left(-\frac{\Delta_\ell}{\lambda}\right)\cdot\int\prod_{i=1}^{N} d\vec{q}_{i_\perp}\, V\left(q^2_{i_\perp}\right)(\cdots), \qquad 12.$$

where $\Delta_\ell = z_{\ell+1} - z_\ell$. We rewrite Equation 11 as

$$\omega\frac{dI}{d\omega} = \frac{\alpha_s}{2\pi^2}\int d\vec{k}_\perp \left\langle 2{\rm Re}\sum_{i=1}^{N}\sum_{j=i+1}^{N}\vec{J}^i_{\rm eff}\cdot\vec{J}^{j\dagger}_{\rm eff}\left(e^{i(\varphi_i-\varphi_j)}-1\right)+\left|\sum_{i=1}^{N}\vec{J}^i_{\rm eff}\right|^2\right\rangle. \qquad 13.$$

This allows us to exhibit the so-called factorization contribution, i.e. the second term in Equation 13, which corresponds to the limit of vanishing phases. This contribution is equivalent to the radiation spectrum induced by a single scattering of momentum transfer $\vec{q}_{\perp_{tot}} = \sum_{i=1}^{N}\vec{q}_i$. It has at most a weak logarithmic medium dependence (21). In what follows, we concentrate on the medium-induced radiation spectrum and drop the factorization term. If we replace sums over i and j with integrals (i.e. we take the sum over scatterings to be arbitrary in number), we obtain the following expression for the spectrum per unit length of the medium in the limit of large N_c:

$$\begin{aligned}\omega\frac{d^2I}{d\omega\, dz} = \frac{\alpha_s N_c}{2\pi^2 L}\int_0^L d\Delta\int_0^{L-\Delta}\frac{dz_1}{\lambda}\int d\vec{U}\\ \cdot\left\langle 2{\rm Re}\sum_{n=0}^{\infty}\vec{J}_1\cdot\vec{J}_{n+2}\left[\exp\left\{i\kappa\sum_{\ell=1}^{n+1}U_\ell^2\frac{\Delta_\ell}{\lambda}\right\}-1\right]\right.\\ \left.\times\,\delta\left(\Delta-\sum_{m=1}^{n+1}\Delta_m\right)\right\rangle, \qquad 14.\end{aligned}$$

with $\vec{U} = \vec{k}_\perp/\mu$ and $\kappa = \lambda\mu^2/2\omega$. In the soft gluon limit, the rescaled emission current is given by

$$\vec{J}_i = \left(\frac{\vec{U}_i}{U_i^2} - \frac{\vec{U}_i+\vec{Q}_i}{(\vec{U}_i+\vec{Q}_i)^2}\right). \qquad 15.$$

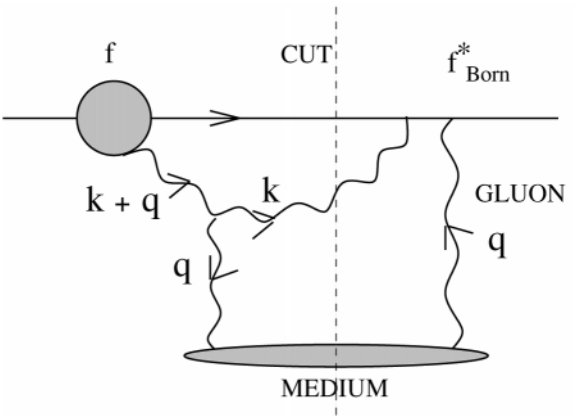

Figure 3 Contribution to the induced gluon spectrum from interference between the amplitude f and the Born amplitude f_{Born}.

Equation 14 exhibits the interference nature and coherent pattern of the spectrum. The phase factor as it appears here can be understood in terms of formation-time arguments, as discussed heuristically in the next section. Moreover, it can be shown (21) that Equation 14 leads to a simple structure of the spectrum per unit length, which is the starting point of Section 3.4:

$$\omega \frac{d^2 I}{d\omega dz} = \frac{\alpha_s N_c}{\pi^2 L} \mathrm{Re} \int_0^L \frac{d\Delta}{\lambda} \int_0^{L-\Delta} \frac{dz_1}{\lambda} \int d\vec{U}\, \vec{f}(\vec{U}, \Delta) \cdot \vec{f}_{\mathrm{Born}}(\vec{U}) \Big|_{\kappa}^{\kappa=0} . \quad 16.$$

Here $\vec{f}_{\mathrm{Born}}(\vec{U})$ is the Born amplitude, defined as

$$\vec{f}_{\mathrm{Born}}(\vec{U}) = \int d\vec{Q}_1\, V\left(Q_1^2\right)\, \vec{J}_1 , \quad 17.$$

and $\vec{f}(\vec{U}, \Delta)$ is the evolved amplitude, which satisfies a Bethe-Salpeter–type equation. Subtracting the contribution for $\kappa = 0$ in Equation 16 corresponds to subtracting the zero-phase contribution in Equation 14. The generic structure of Equation 16 is illustrated in Figure 3. The reader may question the one-gluon exchange approximation used in Figure 3. In fact, the scale of the coupling for each individual scattering is set by the accumulated overall transverse momentum. This justifies the perturbative treatment.

3.2 Heuristic Discussion

In this discussion, we neglect logarithmic and numerical factors of $O(1)$ but keep all relevant parameters. We offer the following semiquantitative argument to explain the coherent pattern of the induced gluon radiation. One defines the formation time of the radiation,

$$t_{\mathrm{form}} \simeq \frac{\omega}{k_\perp^2}, \quad 18.$$

where ω and $k_\perp$ are the gluon energy and transverse momentum (with $\omega \gg k_\perp$ and the typical $k_\perp \simeq \mu$). When $t_{\rm form} \gg \lambda$, radiation takes place in a coherent fashion with many scattering centers acting as a single one. Let us introduce the coherence time (length) $l_{\rm coh}$, which plays an important role in the following considerations. It is associated with the formation time of a gluon radiated by a group of scattering centers that act as a single source of radiation,

$$l_{\rm coh} \simeq \frac{\omega}{\langle k_\perp^2 \rangle_{l_{\rm coh}}}, \qquad 19.$$

with

$$\langle k_\perp^2 \rangle_{l_{\rm coh}} \simeq \frac{l_{\rm coh}}{\lambda}\mu^2 \equiv N_{\rm coh}\mu^2, \qquad 20.$$

assuming a random walk expression for the accumulated gluon transverse momentum. As a consequence, one derives

$$l_{\rm coh} \simeq \sqrt{\frac{\lambda}{\mu^2}\omega}, \qquad 21.$$

and the number of coherent scatterings becomes

$$N_{\rm coh} \simeq \sqrt{\frac{\omega}{\lambda\mu^2}} \equiv \sqrt{\frac{\omega}{E_{\rm LPM}}}, \qquad 22.$$

where the energy parameter $E_{\rm LPM} \equiv \lambda\mu^2$ is introduced (22), in analogy with the QED Landau-Pomeranchuk-Migdal (LPM) phenomenon.

For small $\omega \leq E_{\rm LPM}$, incoherent radiation takes place on L/λ scattering centers. Using the soft ω limit for the single scattering spectrum (23),

$$\frac{\omega dI}{d\omega} \simeq \frac{\alpha_s}{\pi}N_c, \qquad 23.$$

one derives the differential energy spectrum per unit length in the so-called Bethe-Heitler (BH) regime for incoherent radiation:

$$\left.\frac{\omega d^2 I}{d\omega\, dz}\right|_{\rm BH} = \frac{1}{L}\left.\frac{\omega dI}{d\omega}\right|_L \simeq \frac{\alpha_s}{\pi}N_c\frac{1}{\lambda}, \qquad 24.$$

with $l_{\rm coh} \leq \lambda$ and $\omega \leq \omega_{\rm BH} \equiv E_{\rm LPM}$.

The interesting regime of coherent radiation, the LPM regime, is defined by $\lambda < l_{\rm coh} < L$, ($N_{\rm coh} > 1$), i.e.

$$E_{\rm LPM} = \omega_{\rm BH} < \omega < \min\{\omega_{\rm fact}, E\}, \qquad 25.$$

with $\omega_{\rm fact} \sim \frac{\mu^2}{\lambda}L^2$. Because the $N_{\rm coh}$ groups are acting as effective single scattering centers, the energy spectrum is estimated as

$$\left.\frac{\omega d^2 I}{d\omega\, dz}\right|_{\rm LPM} \simeq \frac{1}{l_{\rm coh}}\left.\frac{\omega dI}{d\omega}\right|_{l_{\rm coh}} \simeq \frac{\alpha_s}{\pi}N_c\frac{1}{l_{\rm coh}} \simeq \frac{\alpha_s}{\pi}N_c\sqrt{\frac{\mu^2}{\lambda}\frac{1}{\omega}}. \qquad 26.$$

Comparing Equation 26 with Equation 24, we find a suppression factor given by $\sqrt{E_{\rm LPM}/\omega}$.

For $l_{\rm coh} \geq L$, i.e. when

$$\omega > \omega_{\rm fact} = E_{\rm LPM} \left(\frac{L}{\lambda}\right)^2, \tag{27.}$$

effectively only one scattering center is active (the factorization regime), and correspondingly for $\omega_{\rm fact} < \omega < E$,

$$\left.\frac{\omega d^2 I}{d\omega\, dz}\right|_{\rm fact} \simeq \frac{\alpha_s}{\pi} N_c \frac{1}{L}. \tag{28.}$$

The expressions for the spectrum per unit length in the different regimes (Equations 24, 26, and 28) hold for a medium of finite length $L < L_{cr}$, where

$$L_{cr} = \lambda \sqrt{E/E_{\rm LPM}}, \tag{29.}$$

as derived from the condition that $\omega_{\rm fact} \leq E$ (correspondingly, the condition $E > E_{cr} = E_{\rm LPM}(L/\lambda)^2$ has to be satisfied). A discussion of the radiation spectrum can be found in Reference (21).

In order to obtain the energy loss per unit distance $-dE/dz$, we integrate the gluon spectrum over ω, with $0 \leq \omega \leq E$. In addition to a medium-independent contribution proportional to $\frac{\alpha_s}{\pi} N_c \frac{E}{L}$ (the factorization contribution), we obtain from Equation 26 the medium-induced (LPM) loss, proportional to the size of the medium and given by

$$-dE/dz \simeq \frac{\alpha_s}{\pi} N_c \sqrt{\frac{\mu^2}{\lambda} \omega_{\rm fact}} \simeq \frac{\alpha_s}{\pi} N_c \frac{\mu^2}{\lambda} L \tag{30.}$$

for $L < L_{cr}$. Integrating over z leads to the total loss growing as L^2. For $L > L_{cr}$ (i.e. $E < E_{cr}$), the size does not affect the loss per unit length,

$$-dE/dz \simeq \frac{\alpha_s}{\pi} N_c \sqrt{\frac{\mu^2}{\lambda} E} = \frac{\alpha_s}{\pi} \frac{N_c}{\lambda} \sqrt{E_{\rm LPM} E}. \tag{31.}$$

That is, a dependence proportional to $\sqrt{E}$ is obtained, which is familiar from the QED-coherent LPM suppression (1).

Figure 4 shows the energy loss

$$-\Delta E \equiv \int_0^L -\frac{dE}{dz}\, dz, \tag{32.}$$

for the induced and the factorization cases, as a function of L (N_c is taken to be 1).

Using the random walk expression for the accumulated transverse momentum of the gluon due to successive scatterings in the medium of size L, we find

$$\left\langle k_\perp^2 \right\rangle_L \simeq \mu^2 L/\lambda. \tag{33.}$$

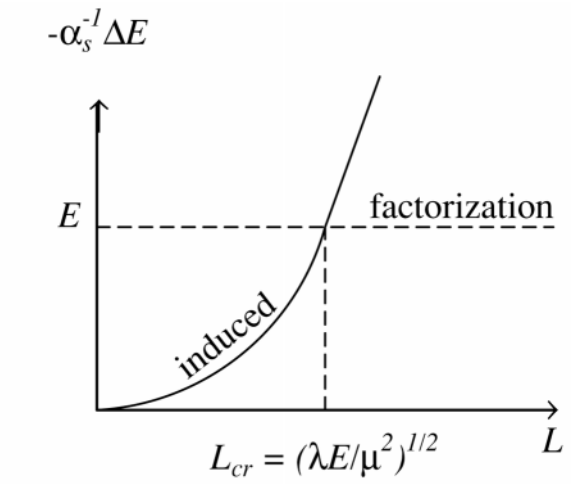

Figure 4 Generic energy loss of a parton as a function of the medium size L.

Inserting this relation in Equation 30, we obtain

$$-dE/dz \simeq \frac{\alpha_s}{\pi} N_c \langle k_\perp^2 \rangle_L. \qquad 34.$$

This relation between the induced energy loss and the jet broadening is independent of the details of the interaction.

3.3 Jet $p_\perp$ Broadening

For the sake of the derivation of the gluon radiative spectrum, let us start with the classical diffusion equation satisfied by the transverse momentum distribution of a high-energy parton that encounters multiple scattering in a medium. Suppose the parton with momentum p is produced in a hard collision with an initial transverse momentum distribution $f_0(U^2)$; U is the dimensionless transverse momentum $\vec{U} \equiv \vec{p}_\perp/\mu$ and $\int d\vec{U}\, f_0(U^2) = 1$.

Neglecting the transverse momentum given to the parton by induced gluon emission, we can derive a kinetic equation for the transverse momentum distribution $f(U^2, z)$ after a distance z in the medium (24).

In terms of the variable $t = z/\lambda_R$, with λ_R the mean free path for a parton of color representation R, we find the following gain-loss equation:

$$\frac{\partial f(U^2,t)}{\partial t} = + \int f(U'^2,t)\, V((\vec{U}' - \vec{U})^2)\, d\vec{U}' - \int f(U^2,t)\, V((\vec{U} - \vec{U}')^2)\, d\vec{U}', \qquad 35.$$

with

$$f(U^2, 0) = f_0(U^2). \qquad 36.$$

Defining $\widetilde{f}(B^2, t)$ as

$$\widetilde{f}(B^2, t) = \int d\vec{U}\, e^{-i\vec{B}\cdot\vec{U}}\ f(U^2, t), \tag{37.}$$

and

$$\widetilde{V}(B^2) = \int d\vec{Q} e^{-i\vec{B}\cdot\vec{Q}}\ V(Q^2), \tag{38.}$$

we find

$$\frac{\partial \widetilde{f}(B^2, t)}{\partial t} = -\frac{1}{4} B^2 \widetilde{v}(B^2)\, \widetilde{f}(B^2, t), \tag{39.}$$

with

$$\widetilde{v}(B^2) \equiv \frac{4}{B^2}[1 - \widetilde{V}(B^2)]. \tag{40.}$$

The characteristic width of the distributions $f(U^2, t)$ is found to be (24)

$$p_{\perp W}^2 = \frac{\mu^2}{\lambda_R} L\ \widetilde{v}(\lambda_R/L). \tag{41.}$$

The linear growth with L is expected and is used to discuss $p_\perp$ broadening of high-energy partons in nuclei. The coefficient $\widehat{q} = \frac{\mu^2}{\lambda}\widetilde{v}$ plays the role of a transport coefficient as encountered in diffusion equations. Equation 41 is equally valid for hot and cold QCD media.

3.4 The Radiative Gluon Energy Spectrum and Induced Energy Loss

Let us now turn to the gluon spectrum.[2] We concentrate on a quark jet. The general case is given in Reference (25). As sketched in Section 3.1 and derived in References (20, 21, 25), the spectrum for the radiated gluon is calculated in terms of the interference term between the quark-gluon amplitude at time t and the complex conjugate Born amplitude. For simplicity, we restrict ourselves here to the case where the quark enters the medium from outside. (An additional term is needed in the case where the quark is produced via a hard scattering at $t = 0$ in the medium). We denote by $f(\vec{U}, \vec{V}, t)$ the quark-gluon amplitude at time t. $\vec{U}$ is the scaled gluon momentum, $\vec{U} \equiv \vec{k}_\perp/\mu$, and $\vec{V} - \vec{U}$ is the scaled quark momentum as illustrated in Figure 5.

To account for the gluon polarization, f is a two-dimensional vector, which is assumed hereafter. The dependence on $\vec{U}$ and $\vec{V}$ is actually only in the combination $\vec{U} - x\vec{V}$ with the momentum fraction $x = k/p$. The amplitude $f(\vec{U}, \vec{V}, t)$ satisfies

[2]For related discussions of gluon bremsstrahlung in dense matter, see also References (26, 27).

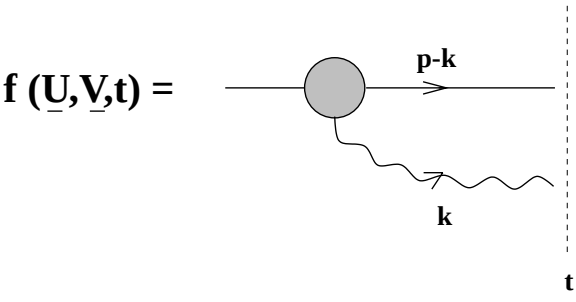

Figure 5 Quark-gluon amplitudes at time t, as discussed in the text.

the initial condition $f(\vec{U}, \vec{V}, 0) = f_{\rm Born}(\vec{U}, \vec{V})$, where $f_{\rm Born}$ is the Born amplitude (to be described shortly).

The induced gluon spectrum is written as

$$\frac{\omega\, d^2I}{d\omega\, dz} = \frac{\alpha_s\, C_F}{\pi^2 L} 2Re \int d\vec{U} \left\{ \int_0^L dt_2 \int_0^{t_2} dt_1 \left[\rho\sigma \frac{N_C}{2C_F} f(\vec{U} - x\vec{V}, t_2 - t_1) \right] \times \left[\rho\sigma \frac{N_C}{2C_F} f^*_{\rm Born}(\vec{U} - x\vec{V}) \right] \right\}_{\omega}^{\omega=\infty}. \quad 42.$$

The various terms in Equation 42 have simple interpretations. The term $\frac{\alpha_S C_F}{\pi^2}$ is the coupling of a gluon to a quark. The term $1/L$ expresses the fact that we calculate the spectrum per unit length of the medium. The factor $\frac{N_c}{2C_F} f(\vec{U} - x\vec{V}, t_2 - t_1)\rho\sigma dt_1$ is the number of scatterers in the medium, $\rho\sigma dt_1$, multiplied by the amplitude for gluon emission at t_1, evolved in time up to t_2, the time of emission in the complex conjugate amplitude. The factor $\frac{N_c}{2C_F} f^*_{\rm Born}(\vec{U} - x\vec{V})\rho\sigma dt_2$ gives the number of scatterers multiplied by gluon emission in the complex conjugate Born amplitude. The subtraction of the value of the integrals at $\omega = \infty$ eliminates the medium-independent zero-phase contribution. Equation 42 may be simplified using $t \equiv (\frac{2C_F}{N_c}\lambda)\tau$. Defining $\tau_0 = \frac{N_c}{2C_F}\frac{L}{\lambda}$, we obtain

$$\frac{\omega d^2 I}{d\omega\, dz} = \frac{\alpha_s N_c}{\pi^2 \lambda} {\rm Re} \int d\vec{Q} \cdot \left\{ \int_0^{\tau_0} d\tau \left(1 - \frac{\tau}{\tau_0}\right) f(\vec{U} - x\vec{V}, \tau) \cdot f^*_{\rm Born}(\vec{U} - x\vec{V}) \right\}_{\omega}^{\omega=\infty}. \quad 43.$$

Owing to the specific dependence of f and $f_{\rm Born}$ on $\vec{U}$ and $\vec{V}$, we can express them in terms of a single impact parameter:

$$f(\vec{U} - x\vec{V}, \tau) = \int \frac{d\vec{B}}{(2\pi)^2} e^{i\vec{B}\cdot(\vec{U} - x\vec{V})} \tilde{f}(\vec{B}, \tau),$$

$$f_{\rm Born}(\vec{U} - x\vec{V}) = \int \frac{d\vec{B}}{(2\pi)^2} e^{i\vec{B}\cdot(\vec{U} - x\vec{V})} \tilde{f}_{\rm Born}(\vec{B}), \quad 44.$$

which allows us to obtain the following expression for the spectrum in impact parameter space:

$$\frac{\omega d^2 I}{d\omega\, dz} = \frac{\alpha_s N_c}{2\pi^3 \lambda} \mathrm{Re} \int \frac{d\vec{B}}{2\pi} \left\{ \int_0^{\tau_0} d\tau \left(1 - \frac{\tau}{\tau_0}\right) \widetilde{f}(\vec{B}, \tau) \cdot \widetilde{f}^*_{\mathrm{Born}}(\vec{B}) \right\}_{\omega}^{\omega=\infty}. \quad 45.$$

The generic diagram appears in Figure 3. Figure 6 shows the complete list of diagrams describing the Born amplitude. Graphs *a–c* in Figure 6 correspond to inelastic reactions with the medium, whereas graphs *d–g* correspond to forward scattering in the medium. For graphs *a–c*, there are corresponding inelastic reactions in the complex conjugate amplitude. In the approximation that the forward elastic amplitude for quark scattering off particles in the medium is purely imaginary, the elastic and inelastic terms are proportional to $V(Q^2)$. The color factors and the expression of each graph contribution are derived in Reference (25).

The quark-gluon amplitude $f(\vec{U}, \vec{V}, t)$ obeys an integral evolution equation derived in References (20, 21, 25). In impact parameter space and in the small-x limit, this equation takes the simple form

$$\frac{\partial}{\partial \tau} \widetilde{f}(\vec{B}, \tau) = i\widetilde{\kappa}\, \nabla_B^2\, \widetilde{f}(\vec{B}, \tau) - 2[1 - \widetilde{V}(B)] \widetilde{f}(\vec{B}, \tau) \quad 46.$$

with $\widetilde{\kappa} = \frac{2C_F}{N_C} \left(\frac{\lambda \mu^2}{2\omega}\right)$ and $\widetilde{f}(\vec{B}, 0) = \widetilde{f}_{\mathrm{Born}}(\vec{B})$. This equation is a Schrödinger-type evolution equation for the propagation of the quark-gluon system in a QCD medium. Comparing Equations 46 and 39 is instructive. The term proportional to $\widetilde{\kappa}$ in Equation 46 is clearly of quantum origin and is associated with the

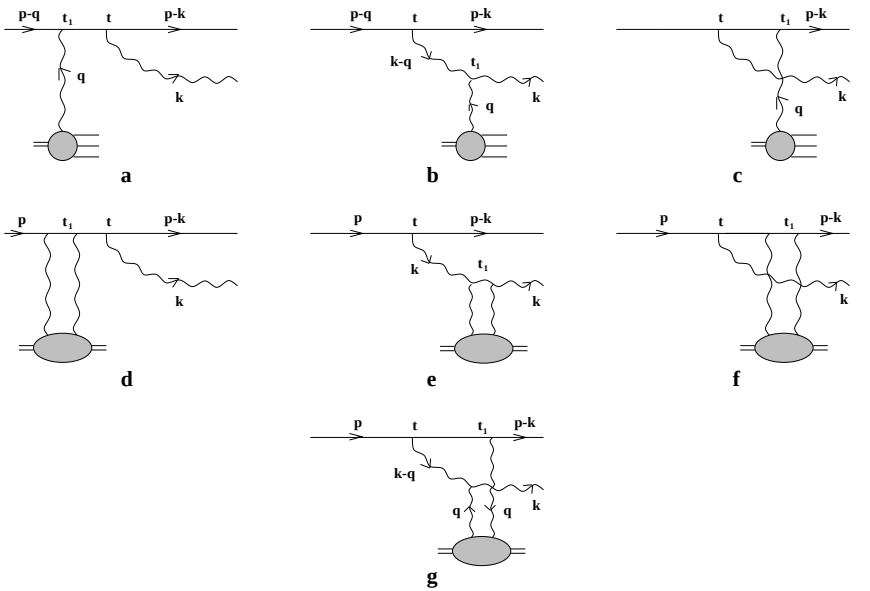

Figure 6 The diagrams contributing to f_{Born}.

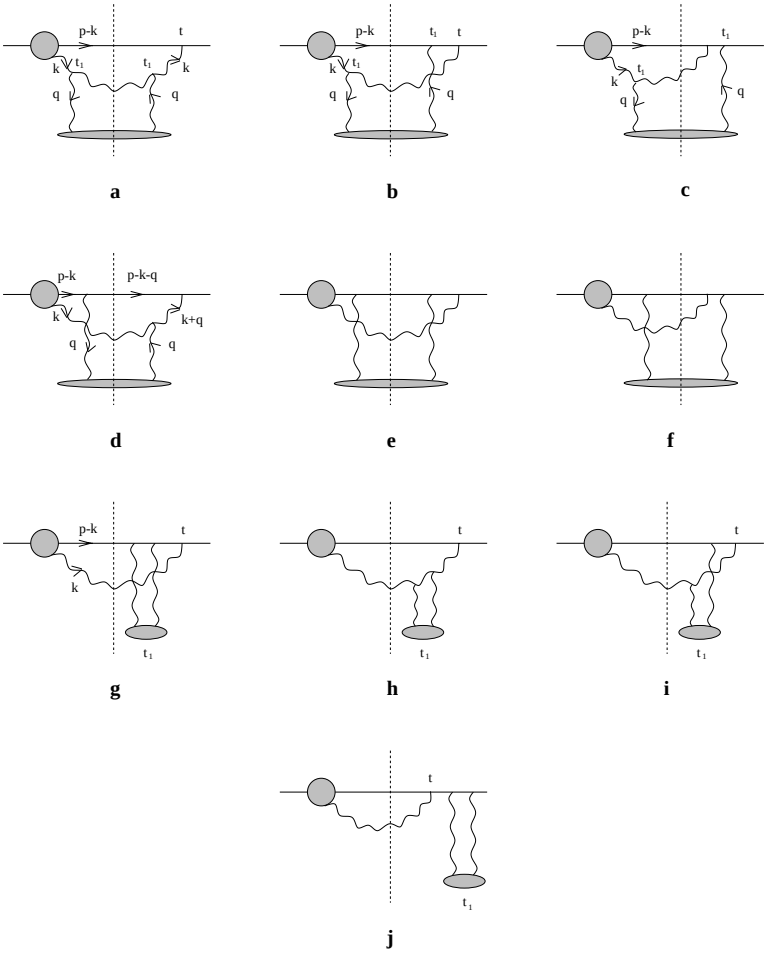

Figure 7 Graphs describing the contributions to the gluon spectrum.

phase of the amplitude, whereas Equation 39 is a classical diffusion equation. Figure 7 depicts the contributions entering the expression for the spectrum (Equation 43).

As long as $\widetilde{v}(B^2) \equiv 4[1 - \widetilde{V}(B)]/B^2$ can be treated as a constant, solving Equation 46 proceeds in analogy with that of the two-dimensional harmonic oscillator with imaginary frequency. We expect that the behavior of $\widetilde{v}(B^2)$ is generally close to the Coulomb potential case, i.e. $\approx \ell n(1/B^2)$ at small B^2. The solution of Equation 46 to logarithmic accuracy is worked out in References (21, 25). In the case where the (quark) jet is produced in matter, one finds for the gluon spectrum

$$\frac{\omega\, d^2I}{d\omega\, dz} = \frac{2\alpha_s C_F}{\pi L}\left[1 - x + \frac{x^2}{2}\right] \ln|\cos(\omega_0 \tau_0)|\,. \qquad 47.$$

From this equation, the energy loss per unit length is derived:

$$-\frac{dE}{dz} = \int_0^\infty \frac{\omega\, d^2I}{d\omega\, dz}\, d\omega \qquad 48.$$

that is, in the small x limit,

$$-\frac{dE}{dz} = \frac{\alpha_s N_c}{4}\,\frac{\mu^2 L}{\lambda}\widetilde{v}\left(\tau_0^{-1}\right). \qquad 49.$$

Notice the remarkable relation (compare Equation 34),

$$-\frac{dE}{dz} = \frac{\alpha_s N_c}{4}\, p_{\perp W}^2, \qquad 50.$$

between energy loss and jet $p_\perp$ broadening (24).

4. PATH INTEGRAL APPROACH

This section presents in some detail a different approach to the LPM effect in QCD, based on the so-called light-cone path integral technique for multiple scattering (28). We refer the reader for derivations and further details to References (29–34). Here we give the essential features of the method by discussing in scalar QED the formalism for an induced transition $a \to bc\,(e \to e'\gamma)$. The interaction Lagrangian is $L_{int} = \lambda[\hat{\psi}_b^\dagger \hat{\psi}_c^\dagger \hat{\psi}_a + h.c.]$. It is assumed that the decay $a \to bc$ does not take place in the vacuum. We later indicate the proper treatment for QCD.

4.1 Derivation of the Basic Formulas

The S-matrix element for the $a \to bc$ transition in an external potential reads

$$\langle bc|\hat{S}|a\rangle = i\int dt d\vec{r}\lambda\psi_b^*(t,\vec{r})\psi_c^*(t,\vec{r})\psi_a(t,\vec{r}), \qquad 51.$$

where ψ_i are the wave functions. Let us consider the case of a static external potential. Then we can write ψ_i as

$$\psi_i(t,\vec{r}) = \frac{1}{\sqrt{2E_i}}\exp[-iE_i(t-z)]\phi_i(z,\vec{\rho}), \qquad 52.$$

where $\vec{\rho}$ is the transverse coordinate, and the function ϕ_i describes the evolution of the ψ_i on the light cone $t - z =$ const. At high energies $E_i \gg m_i$, after substituting Equation 52 into the Klein-Gordon equation, we can obtain for ϕ_i the two-dimensional Schrödinger equation

$$i\frac{\partial\phi_i}{\partial z} = H_i(z)\phi_i, \qquad 53.$$

$$H_i(z) = -\frac{1}{2\mu_i}\left(\frac{\partial}{\partial\vec{\rho}}\right)^2 + e_i U(\vec{\rho},z) + \frac{m_i^2}{2\mu_i}, \qquad 54.$$

where $\mu_i = E_i$, e_i is the electric charge, and U is the potential of the target. Consequently, the values of the ϕ_i at the $\vec{\rho}$ planes $z = z_2$ and $z = z_1$ are related by

$$\phi_i(z_2, \vec{\rho}_2) = \int d\vec{\rho}_1 K_i(\vec{\rho}_2, z_2 \mid \vec{\rho}_1, z_1)\phi_i(z_1, \vec{\rho}_1), \qquad 55.$$

where $K_i(\vec{\rho}_2, z_2 \mid \vec{\rho}_1, z_1)$ is the Green function of the Hamiltonian (Equation 54). Let us introduce the two $\vec{\rho}$ planes located at large distances in front of $(z = z_i)$ and behind $(z = z_f)$ the target. Then, using the convolution relation (Equation 55), we can express the incoming and outgoing wave functions in terms of their asymptotic plane waves at z_i and z_f, respectively. As we show below, this representation turns out to be very convenient for the evaluation of the LPM effect. It is one of the key points of the light-cone path integral approach.

The differential cross section can be written as

$$\frac{d^5\sigma}{dx\, d\vec{q}_b\, d\vec{q}_c} = \frac{2}{(2\pi)^4}\mathrm{Re}\int d\vec{\rho}_1\, d\vec{\rho}_2 \int\limits_{z_1<z_2} dz_1\, dz_2 g F(z_1, \vec{\rho}_1)F^*(z_2, \vec{\rho}_2), \qquad 56.$$

where $F(z, \vec{\rho}) = \phi_b^*(z, \vec{\rho})\phi_c^*(z, \vec{\rho})\phi_a(z, \vec{\rho})$ and $\vec{q}_{b,c}$ are the transverse momenta, x is equal to E_b/E_a, and $g = \lambda^2/[16\pi x(1-x)E_a^2]$ is the vertex factor. Expressing ϕ_i in terms of the asymptotic plane waves, Equation 56 may be represented diagrammatically (Figure 8*a*). We depict $K_i(K_i^*)$ by a right arrow (left arrow). The dotted lines show the transverse density matrix for the initial particle a at $z = z_i$ and the complex conjugate transverse density matrices for the final particles b and c at $z = z_f$. For the spectra integrated over transverse momenta, the relation

$$\int d\vec{\rho}_2 K(\vec{\rho}_2, z_2 \mid \vec{\rho}_1, z_1)K^*(\vec{\rho}_2, z_2 \mid \vec{\rho}_1{}', z_1) = \delta(\vec{\rho}_1 - \vec{\rho}_1{}') \qquad 57.$$

allows us to transform the graph of Figure 8*a* into the ones of Figures 8*b* and 8*c* for the $\vec{q}_c$- and $\vec{q}_{b,c}$-integrated spectra, respectively.

Let us now discuss the $a \to bc$ transition for a random potential of an amorphous target using the representations of Figure 8. In this case, it is appropriate to average the transition cross section over the states of the target. We cannot evaluate analytically the diagrams of Figure 8 for a given state of the target. The basic idea of the approach of References (29, 30, 34) is to represent all the propagators in the

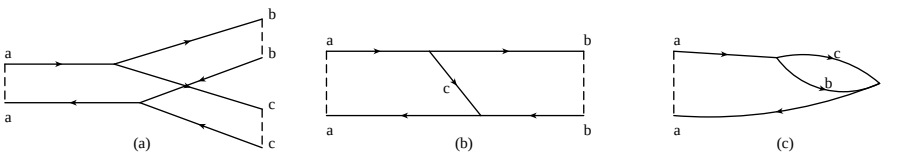

Figure 8 Diagrammatic representation of the $a \to bc$ transition in terms of the two-dimensional Green functions.

path integral form

$$K_i(\vec{\rho}_2, z_2 \mid \vec{\rho}_1 z_1) = \int D\vec{\rho}\, \exp\left\{ i \int dz \left[\frac{\mu_i (d\vec{\rho}/dz)^2}{2} - e_i U(\vec{\rho}, z) \right] - \frac{i m_i^2 (z_2 - z_1)}{2\mu_i} \right\} \qquad 58.$$

and to average over the target states before the integration over the trajectories. It is then remarkable that for the diagrams of Figures 8*b* and 8*c* (and for Figure 8*a* if *b* or *c* has zero charge, say, for the $e \to \gamma e'$ transition), a considerable part of work on the path integration can be done analytically.

Below we consider the $\vec{q}_c$-integrated spectrum. Let z_1 and z_2 be the longitudinal coordinates of the left and right vertices of Figure 8*b*. Taking advantage of the convolution relations (we omit the transverse variables), $K_b(z_f \mid z_1) = K_b(z_f \mid z_2) \otimes K_b(z_2 \mid z_1)$, $K_a^*(z_2 \mid z_i) = K_a^*(z_2 \mid z_1) \otimes K_a^*(z_1 \mid z_i)$, we can divide Figure 8*b* into the initial and final-state interaction two-body parts (denoted by S_c and S_b) and the three-body part (M) located between them. The factors S_i and M are given in terms of the Green functions (Equation 58).

Let us first consider the factor S_i. After averaging over the states of the target, the phase factor

$$\exp\left\{ i e_i \int dz [U(\vec{\rho}, z) - U(\vec{\rho}', z)] \right\} \qquad 59.$$

can be viewed as the Glauber factor for the $i\bar{i}$ pair. Neglecting the correlations in the positions of the medium constituents, we obtain for the averaged value of this phase factor (denoted by $\Phi_i(\{\vec{\rho}\}, \{\vec{\rho}'\})$)

$$\Phi_i(\{\vec{\rho}\}, \{\vec{\rho}'\}) = \exp\left[-\frac{1}{2} \int dz \sigma_{i\bar{i}}(|\vec{\rho}(z) - \vec{\rho}'(z)|) n(z) \right], \qquad 60.$$

where $\{\vec{\rho}\}$ and $\{\vec{\rho}'\}$ are the trajectories for K_i and K_i^*, respectively; $\sigma_{i\bar{i}}$ is the dipole cross section of the interaction with the medium constituent of the $i\bar{i}$ pair; and $n(z)$ is the number density of the target. Then the S_i is given by the path integral $\int D\vec{\rho} D\vec{\rho}' \exp[i\hat{S}_i(\{\vec{\rho}\}, \{\vec{\rho}'\})]$ with the action

$$\hat{S}_i(\{\vec{\rho}\}, \{\vec{\rho}'\}) = \frac{1}{2} \int dz \{ \mu_i [(d\vec{\rho}/dz)^2 - (d\vec{\rho}'/dz)^2] + i\sigma_{i\bar{i}}(|\vec{\rho}(z) - \vec{\rho}'(z)|) n(z) \}. \qquad 61.$$

It is important that the interaction term in Equation 61 depends only on the relative distance between trajectories. This fact allows us to carry out analytically the path integration and obtain a simple formula (28),

$$S_i(\vec{\rho}_2, \vec{\rho}_2', z_2 \mid \vec{\rho}_1, \vec{\rho}_1', z_1) = K_i^0(\vec{\rho}_2, z_2 \mid \vec{\rho}_1, z_1) K_i^{0*}(\vec{\rho}_2', z_2 \mid \vec{\rho}_1', z_1) \Phi_i(\{\vec{\rho}_s\}, \{\vec{\rho}_s'\}), \qquad 62.$$

where

$$K_i^0(\vec{\rho}_2, z_2 \mid \vec{\rho}_1, z_1) = \frac{\mu_i}{2\pi i (z_2 - z_1)} \exp\left[\frac{i\mu_i(\vec{\rho}_2 - \vec{\rho}_1)^2}{2(z_2 - z_1)} - \frac{im_i^2(z_2 - z_1)}{2\mu_i}\right] \quad 63.$$

is the Green function for $U = 0$, and $\{\vec{\rho}_s\}$ and $\{\vec{\rho}'_s\}$ denote the straight line trajectories between $\vec{\rho}_{1,2}$ and $\vec{\rho}'_{1,2}$, respectively. Expression 62 can be obtained by dividing the z interval into steps of small width and taking the multiple integral step by step (28).

The factor M can be treated similarly. The corresponding Glauber factor contains the three-body cross section $\sigma_{\bar{a}bc}$, which depends on the relative transverse separations $\vec{\tau}_{bc} = \vec{\rho}_b - \vec{\rho}_c$ and $\vec{\tau}_{\bar{a}c} = \vec{\rho}_{\bar{a}} - \vec{\rho}_c$ (here and below we view the particle a for a complex conjugate propagator as antiparticle $\bar{a}$). The path integrals can be performed analytically, leading to

$$M(\vec{\rho}_2, \vec{\rho}'_2, z_2 \mid \vec{\rho}_1, \vec{\rho}'_1, z_1) = K_a^0(\vec{R}_2, z_2 \mid \vec{R}_1, z_1) K_a^{0*}(\vec{\rho}'_2, z_2 \mid \vec{\rho}'_1, z_1) \times K_{bc}(\vec{\rho}_2 - \vec{\rho}'_2, z_2 \mid 0, z_1), \quad 64.$$

where $\vec{R}_1 = \vec{\rho}_1$ is the initial coordinate of the center of mass of the bc pair and $\vec{R}_2 = x\vec{\rho}_2 + (1-x)\vec{\rho}'_2$ is its final coordinate. The Green function K_{bc} is given by a path integral on $\vec{\tau}_{bc}$ and describes the evolution of the $bc\bar{a}$ system.

With Equations 62 and 64 it is possible to represent the spectrum for the $a \to bc$ transition for the diagram shown in Figure 8*b* with $\vec{q}_a = 0$ in the following form (34):

$$\frac{d^3I}{dx\, d\vec{q}_b} = \frac{2}{(2\pi)^2} \mathrm{Re} \int d\vec{\tau}_b \exp(-i\vec{q}_b \cdot \vec{\tau}_b) \int_{z_i}^{z_f} dz_1 \cdot \int_{z_1}^{z_f} dz_2\, g\, \Phi_b(\vec{\tau}_b, z_2) K_{bc}(\vec{\tau}_b, z_2 \mid 0, z_1) \Phi_a(\vec{\tau}_a, z_1). \quad 65.$$

Here,

$$\Phi_a(\vec{\tau}_a, z_1) = \exp\left[-\frac{\sigma_{a\bar{a}}(\vec{\tau}_a)}{2} \int_{z_i}^{z_1} dz n(z)\right],$$

$$\Phi_b(\vec{\tau}_b, z_2) = \exp\left[-\frac{\sigma_{b\bar{b}}(\vec{\tau}_b)}{2} \int_{z_2}^{z_f} dz n(z)\right] \quad 66.$$

are the values of the absorption factors for the parallel trajectories, and $\vec{\tau}_a = x\vec{\tau}_b$. The potential for the Green function K_{bc} entering Equations 64 and 65 should be evaluated for parallel trajectories of the center of mass of the bc pair and $\bar{a}$. The resulting Hamiltonian for K_{bc} is given by

$$H_{bc} = -\frac{1}{2\mu_{bc}} \left(\frac{\partial}{\partial \vec{\tau}_{bc}}\right)^2 - \frac{in(z)\sigma_{\bar{a}bc}(\vec{\tau}_{bc}, \vec{\tau}_{\bar{a}c})}{2} + \frac{1}{L_f}, \quad 67.$$

where $\mu_{bc} = E_a x(1-x)$ is the reduced Schrödinger mass, $\vec{\tau}_{\bar{a}c} = x\vec{\tau}_{bc} - \vec{\tau}_a$; the formation length is $L_f = 2E_a x(1-x)/[m_b^2(1-x) + m_c^2 x - m_a^2 x(1-x)]$.

After some algebra, Equation 65 can be rewritten as

$$\frac{d^3I}{dx\,d\vec{q}_b} = \frac{2}{(2\pi)^2}\mathrm{Re}\int d\vec{\tau}_b\,\exp(-i\vec{q}_b\cdot\vec{\tau}_b)\int_{z_i}^{z_f}dz_1\int_{z_1}^{z_f}dz_2$$
$$\cdot\, g\,\{\Phi_b(\vec{\tau}_b,z_2)[K_{bc}(\vec{\tau}_b,z_2\,|\,0,z_1)-K^0_{bc}(\vec{\tau}_b,z_2\,|\,0,z_1)]\Phi_a(\vec{\tau}_a,z_1)$$
$$+[\Phi_b(\vec{\tau}_b,z_2)-1]K^0_{bc}(\vec{\tau}_b,z_2\,|\,0,z_1)[\Phi_a(\vec{\tau}_a,z_1)-1]\} \qquad 68.$$

For a target occupying the region $0 < z < L$, the configurations with $z_{1,2} < 0$ and $z_{1,2} > L$ do not contribute to the cross section. Therefore it is possible to take $z_i = -\infty, z_f = \infty$ in Equation 68.

Integrating over $\vec{q}_b$, we obtain from Equation 68 the x spectrum

$$\frac{dI}{dx} = 2\mathrm{Re}\int_{z_i}^{z_f}dz_1\int_{z_1}^{z_f}dz_2 g\big[K_{bc}(\vec{\rho}_2,z_2\,|\,\vec{\rho}_1,z_1)$$
$$-K^0_{bc}(\vec{\rho}_2,z_2\,|\,\vec{\rho}_1,z_1)\big]\big|_{\vec{\rho}_1=\vec{\rho}_2=0}, \qquad 69.$$

which was derived (29) using the unitarity connection between the probability of the $a \to bc$ transition and the radiative correction to the $a \to a$ transition.

The spectrum (Equation 69) can be represented in another form that demonstrates a close connection between the LPM suppression and Glauber absorption. Treating the second term of the Hamiltonian (Equation 67) as a perturbation, we obtain

$$K_{bc}(0,z_2\,|\,0,z_1) = K^0_{bc}(0,z_2\,|\,0,z_1)+\int_{z_1}^{z_2}d\xi\int d\vec{\rho}\,K^0_{bc}(0,z_2\,|\,\vec{\rho},\xi)v(\xi,\vec{\rho})$$
$$\times K^0_{bc}(\vec{\rho},\xi\,|\,0,z_1)+\int_{z_1}^{z_2}d\xi_1\int_{\xi_1}^{z_2}d\xi_2\int d\vec{\rho}_1\,d\vec{\rho}_2$$
$$\times K^0_{bc}(0,z_2\,|\,\vec{\rho}_2,\xi_2)v(\xi_2,\vec{\rho}_2)\cdot K_{bc}(\vec{\rho}_2,\xi_2\,|\,\vec{\rho}_1,\xi_1)v(\xi_1,\vec{\rho}_1)$$
$$\times K^0_{bc}(\vec{\rho}_1,\xi_1\,|\,0,z_1), \qquad 70.$$

where $v(z,\vec{\rho}) = -n(z)\sigma_{\bar{a}bc}(\vec{\rho},x\vec{\rho})/2$. Taking advantage of Equation 70 we represent Equation 69 in the form

$$\frac{dI}{dx} = \frac{dI^{BH}}{dx}+\frac{dI^{abs}}{dx}, \qquad 71.$$

$$\frac{dI^{BH}}{dx} = T\int d\vec{\rho}\,|\Psi^{bc}_a(x,\vec{\rho})|^2\sigma_{\bar{a}bc}(\vec{\rho},x\vec{\rho}), \qquad 72.$$

$$\frac{dI^{abs}}{dx} = -\frac{1}{2}\mathrm{Re}\int_0^L dz_1 n(z_1)\int_{z_1}^L dz_2 n(z_2)\int d\vec{\rho}\,\Psi^{bc*}_a(x,\vec{\rho})$$
$$\times\sigma_{\bar{a}bc}(\vec{\rho},x\vec{\rho})\,\Phi(x,\vec{\rho},z_1,z_2), \qquad 73.$$

where $T = \int_0^L dz n(z)$ (30). Here

$$\Phi(x, \vec{\rho}, z_1, z_2) = \int d\vec{\rho}\,' K_{bc}(\vec{\rho}, z_2 \mid \vec{\rho}\,', z_1) \Psi_a^{bc}(x, \vec{\rho}\,') \sigma_{\bar{a}bc}(\vec{\rho}\,', x\vec{\rho}\,') \quad 74.$$

is the solution of the Schrödinger equation with the boundary condition

$$\Phi(x, \vec{\rho}, z_1, z_1) = \Psi_a^{bc}(x, \vec{\rho}) \sigma_{\bar{a}bc}(\vec{\rho}, x\vec{\rho}). \quad 75.$$

The first term in Equation 71 corresponds to the impulse approximation. It dominates the cross section in the low-density limit (the Bethe-Heitler regime). The second term describes absorption effects responsible for the LPM suppression.

For a sufficiently thin target, the absorptive correction (Equation 73) can be evaluated neglecting the transverse motion in the $\bar{a}bc$ system inside the target (this corresponds to neglecting the kinetic term in Equation 67). Then, the Green function takes the simple eikonal form

$$K_{bc}(\vec{\rho}_2, z_2 \mid \vec{\rho}_1, z_1) \approx \delta(\vec{\rho}_2 - \vec{\rho}_1) \exp\left[-\frac{\sigma_{\bar{a}bc}(\vec{\rho}_1, x\vec{\rho}_1)}{2} \int_{z_1}^{z_2} dz n(z) \right], \quad 76.$$

and Equations 71–73 give

$$\frac{dI^{fr}}{dx} = 2 \int d\vec{\rho} \left| \Psi_a^{bc}(x, \vec{\rho}) \right|^2 \Gamma_{\bar{a}bc}^{eik}(\vec{\rho}, x\vec{\rho}), \quad 77.$$

with $\Gamma_{\bar{a}bc}^{eik}(\vec{\tau}_{bc}, \vec{\tau}_{\bar{a}c}) = \{1 - \exp[-T\sigma_{\bar{a}bc}(\vec{\tau}_{bc}, \vec{\tau}_{\bar{a}c})/2]\}$. This is the "frozen-size" approximation, which corresponds to the factorization regime discussed in Section 3.

The above analysis is performed for the particle a incident on a target from outside. If it is produced in a hard reaction inside the medium, appropriate modifications are necessary.

4.2 Generalization to the Realistic QED Lagrangian

The generalization of the above analysis to the realistic QED and QCD Lagrangian is simple. Let us consider first the $e \to e'\gamma$ transition in QED. The $\hat{S}$-matrix element can be obtained by replacing λ by $e\bar{u}_{e'}\gamma^\nu \epsilon_\nu u_e$ in Equation 51, where ϵ_ν is the photon polarization vector, and $u_{e'}$ and u_e are the electron spinors (see Reference 32). Since the photon does not interact with the target, we have $\sigma_{\bar{e}\gamma e'}(\vec{\tau}_{\gamma e'}, \vec{\tau}_{\bar{e}e'}) = \sigma(|\vec{\tau}_{\bar{e}e'}|)$, where σ is the dipole cross section for the e^+e^- pair. In terms of the electron-atom differential cross section, $\sigma_{\bar{e}\gamma e'}$ reads

$$\sigma(\vec{\rho}) = \frac{2}{\pi} \int d\vec{q}\,[1 - \exp(i\vec{q} \cdot \vec{\rho})] \frac{d\sigma}{dq^2}. \quad 78.$$

The dipole cross section vanishes as $\vec{\rho} \to 0$, and $\sigma(\vec{\rho})$ factorizes as $\sigma(\vec{\rho}) = C(\rho)\vec{\rho}^{\,2}$, where $C(\rho)$ has a smooth logarithmic dependence at small $\vec{\rho}$ (28, 36).

In the Bethe-Heitler regime, the radiation rate is dominated by $\tau_{\bar{e}e'} < 1/m_e$; for the case of strong LPM suppression, the typical values of $\tau_{\bar{e}e'}$ are even smaller. One can approximate the Hamiltonian (Equation 67) by the harmonic oscillator Hamiltonian and obtain from Equation 69 the radiation rate per unit length. In an infinite medium, in the regime of strong LPM suppression, the radiation rate per unit length takes the form

$$\frac{d^2I}{dx\,dz} \approx \frac{\alpha[4-4x+2x^2]}{2\pi}\sqrt{\frac{C(\rho_{\rm eff}x)}{2x(1-x)E_e}}. \qquad 79.$$

The value of $\rho_{\rm eff}$ can be estimated as $\rho_{\rm eff} \sim (2L'_f/\mu_{\gamma e'})^{1/2}$, where the formation length L'_f is the typical value of $|z_2 - z_1|$ in Equation 69. For strong suppression, $\rho_{\rm eff}$ becomes much smaller than $1/m_e x$, the characteristic transverse size in the Bethe-Heitler regime. For this reason, the spectrum for strong suppression (Equation 79) is insensitive to the electron mass (35). Note that the oscillator approximation is equivalent to the Fokker-Planck approximation in momentum representation used in Migdal's analysis (2). This is not surprising, since within logarithmic accuracy, $\sigma(\rho) \propto \vec{\rho}^{\,2}$ leads to a Gaussian diffusion of the electron in transverse momentum space (28). This feature underlies the relationship given in Section 3 relating the energy loss and $p_\perp$ broadening in QCD.

For an accurate numerical evaluation of the LPM effect, it is convenient to use the form given by Equations 71–73. In References (30, 33), this form is used for the analysis of the recent data on bremsstrahlung from high-energy electrons taken by the E-146 SLAC collaboration (3). Excellent agreement (at the level of the radiative corrections) with the data is found.

4.3 Induced Gluon Emission in QCD

We now discuss the induced gluon emission from a fast quark in QCD. At the level of the radiation cross section, involving the sum over states of the medium, we can formulate the theory much as we did in the QED case. The path integral representations for the diagrams of Figure 8 can be written by introducing into the vacuum path integral formulas the Glauber factors for propagation of the color-neutral partonic systems. The quark trajectory for the complex conjugate amplitude can be regarded as that of an antiquark with negative kinetic and mass terms. It follows from the relation $-T_q^* = T_{\bar{q}}$ (here T_q and $T_{\bar{q}}$ represent the color generators for a quark and an antiquark). The $q\bar{q}$, gg, $q\bar{q}g$ configurations that can appear in graphs like those of Figures 8*b* and 8*c* have only one color-singlet state. The diffraction operator has only diagonal matrix elements involving the two-body cross sections $\sigma_{q\bar{q}}(\vec{\rho})$, $\sigma_{gg}(\vec{\rho}) = \frac{9}{4}\sigma_{q\bar{q}}(\vec{\rho})$, and the three-body cross section $\sigma_{gq\bar{q}}(\vec{\rho}_{gq}, \vec{\rho}_{\bar{q}q}) = \frac{9}{8}[\sigma_{q\bar{q}}(|\vec{\rho}_{gq}|)+\sigma_{q\bar{q}}(|\vec{\rho}_{g\bar{q}}|)]-\frac{1}{8}\sigma_{q\bar{q}}(|\vec{\rho}_{q\bar{q}}|)$ (36). Thus, the spectra integrated over quark or/and gluon transverse momenta can be evaluated like the $a \to bc$ transition in QED discussed above, with all the particles now being charged (colored).

In order to calculate the x spectrum (Equation 69), one takes $\vec{\rho}_{\bar{q}q} = x\vec{\rho}_{gq}$, and writes the three-body cross section as $\sigma_{gq\bar{q}}(\vec{\rho}_{gq}, x\vec{\rho}_{gq}) = \frac{9}{8}[\sigma_{q\bar{q}}(\rho) + \sigma_{q\bar{q}}((1-x)\rho)] - \frac{1}{8}\sigma_{q\bar{q}}(x\rho)$, where $\rho = |\vec{\rho}_{gq}|$. As in QED, the spectrum can be estimated using the oscillator parameterization $\sigma_{gq\bar{q}}(\vec{\rho}, x\vec{\rho}) \approx C_3(x)\vec{\rho}^{\,2}$, where $C_3(x) = \frac{1}{8}\{9[1+(1-x)^2] - x^2\}C_2(\rho_{\text{eff}})$, $C_2(\rho_{\text{eff}}) = \sigma_{q\bar{q}}(\rho_{\text{eff}})/\rho_{\text{eff}}^2$. Here ρ_{eff} is the typical size of the $q\bar{q}g$ system dominating the radiation rate, which in the limit of strong LPM suppression, takes the form

$$\frac{d^2I}{dx\,dz} \approx \frac{\alpha_s(4-4x+2x^2)}{3\pi}\sqrt{\frac{2nC_3(x)}{E_q x^3(1-x)}}. \qquad 80.$$

Ignoring the contributions to the energy loss from the two narrow regions near $x \approx 0$ and $x \approx 1$ in which Equation 80 is not valid, we find the energy loss per unit length

$$\frac{d\Delta E_q}{dz} \approx 1.1\alpha_s\sqrt{nC_3(0)E_q}, \qquad 81.$$

where to logarithmic accuracy $\rho_{\text{eff}} \sim [\alpha_s^2 nE_q x(1-x)]^{-1/4}$ is used. Note that, as in QED, the elimination of the infrared divergence for strong suppression is a direct consequence of the medium modification of the gluon formation length, which makes the typical transverse distances much smaller than $1/m_{g,q}$.

The medium modification of the formation length plays an important role in the case of gluon emission by a quark produced inside a medium. In this case, finite-size effects become important and suppress the radiation rate (see Equation 47). This finite-size suppression leads to the L^2 dependence of the energy loss for a high-energy quark (Equation 49). We obtain

$$\Delta E_q \sim \alpha_s C_3(0) n L^2. \qquad 82.$$

This regime holds as long as $L \leq (E_q/nC_3(0))^{1/2}$. Then it transforms into the $\Delta E_q \propto L$ behavior given by Equation 81. More detailed discussions and numerical estimates are given in References (31) and (32), where, in addition to the $q \to gq$ transition, the $g \to gg$ transition is considered in an analogous way.

4.4 Comparison with the BDMPS Approach

We conclude this section with a short comment on the connection between the path integral approach and the approach discussed in Section 3, known as the BDMPS approach (after the names of the authors of Reference 21).

Let us consider the case of a parton entering the medium from outside. The equivalence of the two approaches may be established in the zero-mass case using Equations 71–73 along with Equation 77. As mentioned above, the frozen-size expression (Equation 77) corresponds to the factorization contribution. This is

neglected in the BDMPS approach because of its weak medium dependence, as discussed in Section 3.1.

Rewriting Equation 71 as

$$\frac{dI}{dx} = \frac{dI^{abs}}{dx} + \frac{dI^{fr}}{dx} - \left(\frac{dI^{fr}}{dx} - \frac{dI^{BH}}{dx}\right), \qquad 83.$$

and ignoring the second term, we can show that

$$\frac{dI}{dx} = \frac{dI^{abs}}{dx}\bigg|_{\omega=\infty}^{\omega}, \qquad 84.$$

and can identify in Equation 73 the product $\Psi_a^{bc}\sigma_{\bar{a}bc}$ and Φ with the amplitudes f_{Born} and f, respectively, which are discussed in Section 3.

For the case of a parton produced inside a medium, similar arguments lead again to the equivalence of the two approaches. Further details can be found in Reference (25).

5. RADIATIVE ENERGY LOSS IN AN EXPANDING QCD PLASMA

In the previous sections we have discussed the suppression of gluon radiation owing to multiple scatterings of energetic partons propagating through dense matter with properties that are constant in time.

Here we consider the case of a parton of high energy E traversing an expanding hot QCD medium. We concentrate on the induced gluon radiation and the resulting energy loss of a quark (37, 38).

Let us imagine the medium to be a QGP produced in a relativistic central nucleus-nucleus collision, which occurs at (proper) time $t = 0$. We have in mind the realistic situation where a quark is produced by a hard scattering within the (not yet thermalized) medium, and at time t_0 it enters the homogeneous plasma at high temperature T_0. The plasma expands longitudinally with respect to the collision axis. We label the thermalization time t_0, and for most of the results, the limit $t_0 \to 0$ may be taken with impunity. The quark, for simplicity, is assumed to propagate in the transverse direction with vanishing longitudinal momentum, i.e. at rapidity $y = 0$, such that its energy is equal to its transverse momentum. On its way through the plasma, the quark hits layers of matter that are cooled down by the longitudinal expansion. It is assumed that the plasma lives long enough that the quark is able to propagate a given distance L within the quark-gluon phase of matter.

As a consequence of the medium expansion, the parton propagation in the transverse direction is affected by the position-dependent density of the plasma $\rho(z)$ and the parton cross section $d^2\sigma/d^2\vec{q}_\perp(\vec{q}_\perp, z)$, where z denotes the distance that the quark has propagated through the plasma. Therefore, the screening mass μ

and the mean free path λ both depend on z. When the properties of the expanding plasma are described by the hydrodynamical model proposed by Bjorken (39), the scaling law

$$T^3 t^\alpha = \text{const} \qquad 85.$$

applies, where the (proper) time t at rapidity $y = 0$ coincides with z. The power α, approximated below by a constant, has values between 0 and 1 for an ideal fluid.

Correspondingly, the transport coefficient $\hat{q}(t)$ defined as

$$\hat{q}(t) \simeq \rho(t) \int d^2\vec{q}_\perp \vec{q}_\perp^{\,2} \frac{d\sigma}{d^2\vec{q}_\perp} = \frac{\mu^2(t)}{\lambda(t)} \tilde{v} \qquad 86.$$

becomes time dependent and satisfies

$$\hat{q}(t) = \hat{q}(t_0) \left(\frac{t_0}{t}\right)^\alpha, \qquad 87.$$

because of Equation 85. As a result (37), the radiative energy loss ΔE for the quark produced inside the medium and traversing an expanding medium is

$$-\Delta E = \frac{2}{2-\alpha} \frac{\alpha_s N_c}{4} \hat{q}(L) L^2. \qquad 88.$$

In the high-temperature phase of QCD matter (reviewed in Reference 10),

$$1 - \alpha = O\left[\alpha_s^2(T)\right]. \qquad 89.$$

The coefficient $\hat{q}(L) = \hat{q}[T(L)]$ must be evaluated at the temperature, $T(L)$, that the quark finally "feels" after it has passed the distance L through the medium, which during this propagation cools down to $T(L)$. It is possible to take the limit $\alpha = 1$ for an expanding ideal relativistic plasma. In this limit, the maximal loss is achieved. It is twice as large as the corresponding static case at fixed temperature $T(L)$.

So far we have discussed the result for the case of $E > E_{cr}(L)$, actually taking $E \to \infty$. In Reference (38), the approach of the quark energy loss ΔE to this limit is studied numerically as a function of the quark energy E. One finds that, e.g. with $L = 6$ fm, the radiative energy loss is independent of energy E when $E > 100$ GeV $\simeq E_{cr}$, as indicated by Equation 88.

In summary, we do of course expect the energy loss in an expanding medium to be larger than in the static case evaluated at the final temperature, since the parton passes through hotter layers during the early phase of the expansion. Perhaps the surprising feature is that the enhancement factor does not depend on the initial temperature T_0. This result must be related to the coherence pattern of the medium-induced radiation. The emission of gluons contributing to the energy loss requires a finite time, which reduces the effects of the early stages of the QGP expansion.

6. INDUCED ENERGY LOSS OF A HARD QUARK JET IN A FINITE CONE

Let us now consider a typical calorimetric measurement of hard jets produced in heavy-ion collisions (40). The consequence of a large energy loss is the attenuation of the spectrum, usually denoted as jet quenching. It is necessary to study the angular distribution of radiated gluons in order to give quantitative predictions for the energy lost by a jet traversing hot matter. Only the gluons radiated outside the cone defining the jet contribute to the energy loss.

The calculation of the angular distribution is discussed in References (34, 41), and (42) for a hard jet produced in the medium. Here we have in mind a hard quark jet of high energy E produced by a hard scattering in a dense QCD medium and propagating through it over a distance L. Following Reference (41), we concentrate on the integrated loss outside an angular cone of opening angle $\theta_{\rm cone}$ (Figure 9),

$$-\Delta E(\theta_{\rm cone}) = L \int_0^\infty d\omega \int_{\theta_{\rm cone}}^{\pi} \frac{\omega d^3 I}{d\omega\, dz\, d\theta}\, d\theta. \qquad 90.$$

In the following, we consider the normalized loss by defining the ratio

$$R(\theta_{\rm cone}) = \frac{\Delta E(\theta_{\rm cone})}{\Delta E}. \qquad 91.$$

This ratio $R(\theta_{\rm cone})$ turns out to depend on just one single dimensionless variable

$$R = R(c(L)\theta_{\rm cone}), \qquad 92.$$

where

$$c^2(L) = \frac{N_c}{2C_F}\hat{q}\,(L/2)^3. \qquad 93.$$

The "scaling behavior" of R means that the medium and size dependences are universally contained in the function $c(L)$, which is a function of the transport

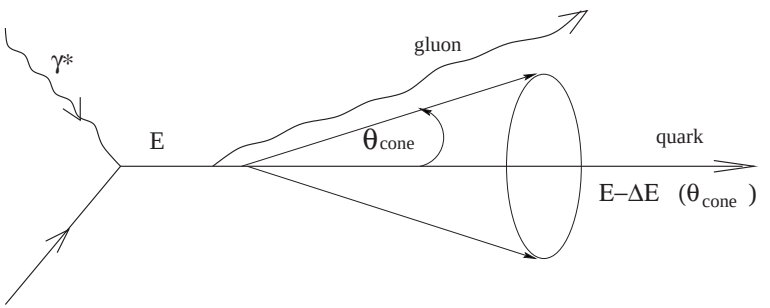

Figure 9 Example of a hard process producing a quark jet. The gluon is emitted outside the cone with angle $\theta_{\rm cone}$.

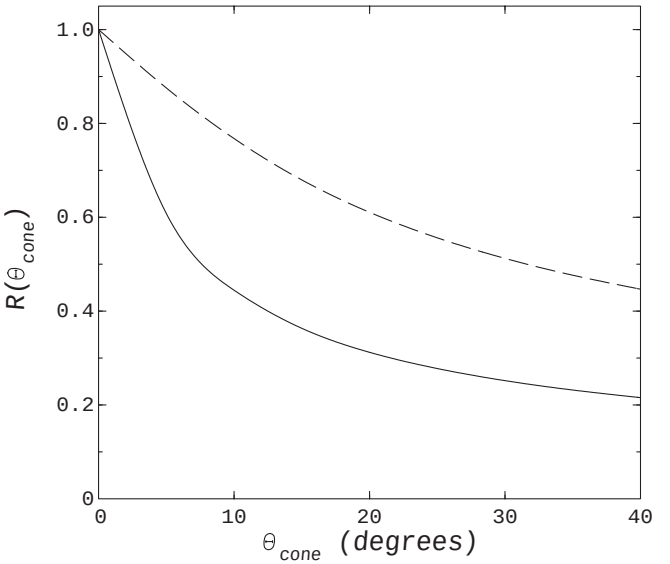

Figure 10 Medium-induced (normalized) energy loss distribution as a function of cone angle θ_{cone} for hot ($T = 250$ MeV) (solid curve) and cold matter (dashed curve) at fixed length $L = 10$ fm.

coefficient $\hat{q}$ and of the length L, as defined by Equation 93. Figure 10 shows the variation of R with θ_{cone}. The ratio $R(\theta_{\text{cone}})$ is also universal in the sense that it is the same for an energetic quark as for a gluon jet. The fact that θ_{cone} scales as $1/c(L)$ may be understood from the following physical argument (22): The radiative energy loss of a quark jet is dominated by gluons having $\omega \simeq \hat{q}L^2$. The angle between the emitted gluon and the quark is $\theta \simeq k_\perp/\omega$, and $k_\perp^2 \simeq \hat{q}L$, so the typical gluon angle is $\theta^2 \simeq 1/\hat{q}L^3$.

Thus far we have discussed the medium-induced energy loss. To consider the total energy loss of a jet of a given cone size, it is important to take into account the medium-independent part. For a quark jet in a cone, this may be estimated as (41)

$$-\Delta E^{fact}(\theta_{\text{cone}}) \simeq \frac{4}{3}\frac{\alpha_s C_F}{\pi} E \ln\left(\frac{\theta_{\max}}{\theta_{\text{cone}}}\right), \qquad 94.$$

using a constant α_s [$\theta_{\max}$ is taken $\mathcal{O}(\pi/2)$].

7. PHENOMENOLOGICAL IMPLICATIONS

We now work out orders-of-magnitude estimates for the radiative induced energy loss. To do so we need to specify the value of the transport coefficient $\hat{q}$, which controls its magnitude. The following numbers are obtained for a quark jet produced in matter.

For hot matter at $T = 250$ MeV, with $\frac{\mu^2}{\lambda} \sim 1$ GeV/fm^2 taken from perturbative estimates and a typical value for $\tilde{v} \approx 2.5$, we find $\hat{q} \simeq 0.1$ GeV^3 (24). With $\alpha_s = \frac{1}{3}$, this makes the total energy loss

$$-\Delta E \approx 60 \text{ GeV } \left(\frac{L}{10 \text{ fm}}\right)^2. \qquad 95.$$

Reference (24) shows that for cold nuclear matter, it is possible to relate $\hat{q}$ to the gluon structure function G evaluated at an average scale $\mu^2 \frac{\lambda}{L}$, actually

$$\hat{q} \simeq \frac{2\pi^2 \alpha_s}{3} \rho \, [xG(x)]. \qquad 96.$$

Taking the nuclear density $\rho \sim 0.16$ fm^{-3}, $\alpha_s = \frac{1}{2}$, and $xG \sim 1$ for $x < 0.1$, it is found that

$$-\Delta E \approx 4 \text{ GeV } \left(\frac{L}{10 \text{ fm}}\right)^2. \qquad 97.$$

These values do suggest that hot matter may be effective in stimulating significant radiative energy loss of high-energy partons. As discussed in Section 5, the energy loss is even larger in an expanding hot medium than in the corresponding static one.

Next we turn to the medium-induced energy loss $-\Delta E(\theta_{\text{cone}})$ for energetic jets. We may use the estimates above to give orders of magnitude for $c(L)$ in the case of hot and cold media:

$$c(L)_{\text{hot}} \simeq 40 \, (L/10 \text{ fm})^{3/2}.$$

A much smaller value is found for cold nuclear matter:

$$c(L)_{\text{cold}} \sim 10 \, (L/10 \text{ fm})^{3/2}.$$

As expected from the fact that the normalized loss $R(\theta_{\text{cone}})$ depends universally on $c(L)\theta_{\text{cone}}$, Figure 10 shows that the jets are more collimated in the hot medium than in the cold one. The loss is, however, still appreciably large even for cone sizes of order $\theta_{\text{cone}} \simeq 30^\circ$. Again, keeping in mind that the estimates are based on the leading logarithmic approximation, we show in Figure 11 the variation of $\Delta E(\theta_{\text{cone}})$ with θ_{cone} of the medium-induced (for a hot medium with $T = 250$ MeV) and the medium-independent energy losses.

We now offer a few examples of phenomena that are sensitive to parton energy loss in dense matter. Presently available experimental results can be instructive for the future measurements at higher energies.

As a projectile traverses dense nuclear matter, the width of the transverse momentum distribution of partons increases. pA and AA scattering allow experimental study of parton $p_\perp$ broadening for the initial quarks in the Drell-Yan process and for gluons in J/Ψ production, respectively (see e.g. References 43, 44). Recent analysis of the J/Ψ data does indeed show $p_\perp$ broadening of the initial gluon.

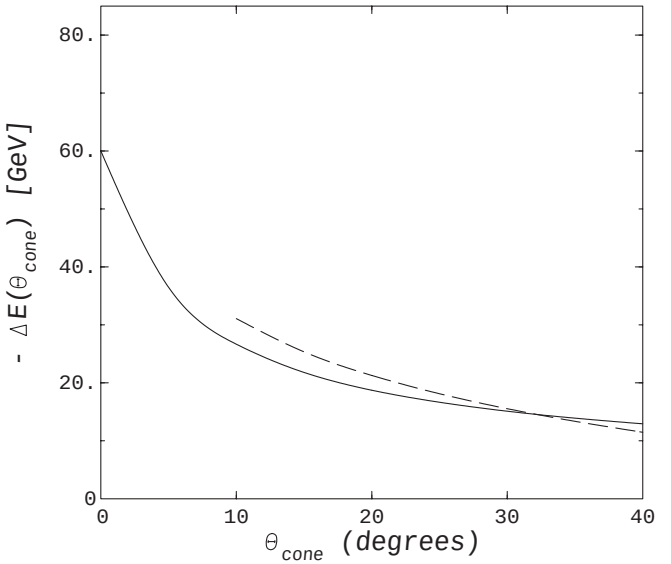

Figure 11 Energy loss in a hot medium at $T = 250$ MeV, as a function of θ_{cone}. The dashed curve represents the medium-independent part of energy loss for $E = 250$ GeV. $L = 10$ fm.

When expressed in terms of the ratio $\hat{q}/\rho$, this leads to $\hat{q}/\rho = 9.4 \pm 0.7$ (45). In the absence of strong final-state effects, this is consistent with the prediction obtained from Equation 96 with $\alpha_s \approx 1/2$ and $xG(x) \approx 1$.

These processes also contain information on the energy loss in the initial state due to matter effects (46, 47). In the Drell-Yan process, the observed energy loss $-\Delta E$ of the incident quarks is indeed compatible with the estimate given in Equation 97, including the L^2 dependence, as measured and analyzed in Reference (48).

Large $p_\perp$ particle and jet spectra and production rates in high-energy collisions are especially sensitive to a finite energy loss, since the partons are propagating through a long-lived high-density medium before hadronization occurs. Under extreme conditions the jets may even be destroyed before emerging from the medium (7). However, hadron spectra from present experiments of pp, pA, and AA collisions, mainly from the CERN SPS, show no strong evidence of suppression (49, 50). This result, which is obscured by large theoretical uncertainties, may indicate that at present energies the lifetime of the dense partonic matter is shorter than the mean free path of the propagating partons. Significant jet quenching should become clearly observable in nucleus-nucleus collisions at RHIC and higher energies, even for transverse momenta as low as $p_\perp \geq 3$ GeV. References (51) and (52) comment on the magnitude of the predicted jet quenching. Suppression of hadronic $p_\perp$ distributions in the case of a thin plasma, which allows only a small number (≤ 3) of scatterings, is analyzed in Reference (53).

Jet quenching for very energetic jets is also discussed in References (40, 54), and (55). In particular, the ratio of monojets to dijets that can be observed in ultrarelativistic heavy-ion collisions is predicted by theory.

A further interesting proposal for studying the modification of jet fragmentation due to energy loss is that of References (56) and (57). Noting that photons are essentially unaffected by the hadronic medium, these authors propose to measure the charged-particle $p_\perp$ distribution in the transverse direction opposite to a tagged photon, i.e. in $\gamma +$ jet events of high-energy heavy-ion collisions. With increased luminosity, this may even be possible at RHIC energies.

Relevant information about dense hadronic matter produced in collisions is related to dileptons from final heavy-meson decays (58). Shuryak (59) pointed out the importance of the energy loss of charm and bottom quarks owing to their interactions in the medium. In the extreme case, they may even be stopped in dense matter. Assuming, for example, that the charmed mesons D and D^* take all the charm quark momentum in the fragmentation process, the final leptons from the semileptonic decay populate the invariant dilepton mass spectrum at masses below 1 to 2 GeV (4 to 5 GeV for bottom decays); as a result, dilepton spectra in nucleus-nucleus collisions for invariant masses above 2 GeV are not dominated by correlated semileptonic charm and bottom decays. This expected strong suppression due to energy loss is confirmed by further detailed (Monte Carlo) studies (60–62).

8. OUTLOOK

This review has described recent theoretical results related to energy loss and $p_\perp$ broadening of a high-energy quark or gluon (jet) traversing QCD media. Phenomenological implications for measurements in both cold and hot (QGP) matter have been discussed. The orders of magnitude predicted for the energy lost by an energetic jet in hot deconfined matter underline the significance of the corresponding measurements as specific signals.

There remain a couple of important open questions triggered by the coherent character of the induced energy loss. One is related to the formulation of a transport model (Monte Carlo) that correctly simulates the interference pattern of gluon radiation induced by multiple scattering (18, 22). It is indeed crucial, when calculating rates for processes leading to thermal and chemical equilibration of partons, to include medium effects (63–69). In the same context, it is important to properly take into account the influence of the LPM effect on the production of dileptons and real photons produced in a QGP or in a hadron gas (70). In any case, the partons are not very energetic, since their energies are of the order of the plasma temperature. This renders invalid the asymptotic treatment that was used above.

We have already mentioned that our numerical estimates give only orders of magnitude, since they are obtained in leading order in the QCD coupling. The main aim of the present theoretical treatments is therefore to encourage

experimentalists at RHIC, and later at LHC, to carefully explore heavy-quark production and especially jet phenomena in ultra-relativistic heavy-ion collisions (71). High-$p_\perp$ nuclear physics may become an exciting new frontier at these colliders (52) because of the possible jet extinction or crucial modifications of the spectra (7) due to medium effects. The best guiding example comes from the long-term study of hard jets in hadron-hadron scattering, from the first evidence at the CERN ISR, to the analysis of jet cross sections at transverse momenta of $p_\perp \simeq 500$ GeV at CDF and DØ, which has been successfully carried out by an active interplay between experiments and perturbative QCD (72).

Medium effects will continue to attract increasing attention, and we hope that eventually the predicted suppression mechanism will be demonstrated by future experiments in a convincing manner. More detailed treatments and improvements to the theory are certainly necessary to complete this program. It constitutes an important chapter of what has been called (73) the health report of QCD.

ACKNOWLEDGMENTS

RB and DS are grateful for the pleasant and fruitful collaboration with Yu L Dokshitzer, AH Mueller, and S Peigné on the various aspects of these topics during the past few years. We thank M Dirks, IP Lokhtin, D Denegri, K Redlich, H Satz, E Shuryak, and A Smilga for valuable comments and discussions. Partial support by the Deutsche Forschungsgemeinschaft under contract Ka 1198/4-1 is acknowledged.

LITERATURE CITED

1. Landau LD, Pomeranchuk IY. *Dokl. Akad. Nauk SSSR* 92:535, 735 (1953)
2. Migdal AB. *Phys. Rev.* 103:1811 (1956)
3. Anthony PL, et al (E-146 SLAC Collaboration). *Phys. Rev. Lett.* 75:1949 (1995); *Phys. Rev. D* 56:1373 (1997)
4. Klein S. *Rev. Mod. Phys.* 71:1501 (1999)
5. Jackson JD. *Classical Electrodynamics*. p. 618. New York: Wiley (1975)
6. Ter-Mikaelian ML. *High Energy Electromagnetic Processes in Condensed Media*. New York: Wiley (1972)
7. Bjorken JD. Fermilab publication Pub-82/59-THY, Batavia (1982); Erratum, unpublished
8. Thoma MH. *Quark-Gluon Plasma 2*, ed. RC Hwa, p. 51. Singapore: World Sci. (1995)
9. LeBellac M. *Thermal Field Theory*. Cambridge, UK: Cambridge Univ. Press (1996)
10. Nieto A. *Int. J. Mod. Phys.* A12:1431 (1997)
11. Braaten E, Pisarski RD. *Phys. Rev. Lett.* 64:1338 (1990); Braaten E, Pisarski RD. *Nucl. Phys.* B337:569 (1990); *Nucl. Phys.* B399:310 (1990)
12. Frenkel J, Taylor JC. *Nucl. Phys.* B334:199 (1990)
13. Braaten E, Thoma MH. *Phys. Rev. D* 44:R2625 (1991)
14. Thoma MH. *Phys. Lett.* B273:128 (1991)

15. Mustafa MG, Pal D, Srivastava DK. *Phys. Rev.* C57:889 (1998)
16. Baier R, Dirks M, Redlich K. hep-ph/9910353 (1999)
17. Casher A, Neuberger H, Nussinov S. *Phys. Rev. D* 20:179 (1979); Kopeliovich BZ, Niedermayer F. *Yad. Fiz.* 42:797 (1985)
18. Gyulassy M, Wang XN. *Nucl. Phys.* B420:583 (1994)
19. Wang XN, Gyulassy M, Plümer M. *Phys. Rev. D* 51:3436 (1995)
20. Baier R, Dokshitzer YL, Peigné S, Schiff D. *Phys. Lett.* B345:277 (1995)
21. Baier R, et al. *Nucl. Phys.* B483:291 (1997)
22. Dokshitzer YL. *Nucl. Phys.* A638:291c (1998)
23. Gunion JF, Bertsch G. *Phys. Rev. D* 25:746 (1982)
24. Baier R, et al. *Nucl. Phys.* B484:265 (1997)
25. Baier R, Dokshitzer YL, Mueller AH, Schiff D. *Nucl. Phys.* B531:403 (1998)
26. Knoll J, Voskresensky DN. *Ann. Phys.* 249:532 (1996)
27. Kovchegov YV, Mueller AH. *Nucl. Phys.* B529:451 (1998)
28. Zakharov BG. *Sov. J. Nucl. Phys.* 46:92 (1987)
29. Zakharov BG. *JETP Lett.* 63:952 (1996)
30. Zakharov BG. *JETP Lett.* 64:781 (1996)
31. Zakharov BG. *JETP Lett.* 65:615 (1997)
32. Zakharov BG. *Phys. Atom. Nucl.* 61:838 (1998)
33. Zakharov BG. *Phys. Atom. Nucl.* 62:1008 (1999)
34. Zakharov BG. *JETP Lett.* 70:176 (1999); hep-ph/9906373 (1999)
35. Baier R, et al. *Nucl. Phys.* B478:577 (1996)
36. Nikolaev NN, Zakharov BG. *JETP* 78:598 (1994)
37. Baier R, Dokshitzer YL, Mueller AH, Schiff D. *Phys. Rev.* C58:1706 (1998)
38. Zakharov BG. hep-ph/9807396 (1998)
39. Bjorken JD. *Phys. Rev. D* 27:140 (1983)
40. Lokhtin IP, Snigirev AM. *Phys. Lett.* B440:163 (1998)
41. Baier R, Dokshitzer YL, Mueller AH, Schiff D. *Phys. Rev.* C60:064902 (1999)
42. Wiedemann UA, Gyulassy M. *Nucl. Phys.* B560:345 (1999)
43. Gavin S, Gyulassy M. *Phys. Lett.* B214:241 (1988)
44. Hüfner J, Kurihara Y, Pirner HJ. *Phys. Lett.* B215:218 (1988)
45. Kharzeev D, Nardi M, Satz H. *Phys. Lett.* B405:14 (1997)
46. Brodsky JS, Hoyer P. *Phys. Lett.* B298:165 (1993)
47. Nagle JL, Bennett MJ. *Phys. Lett.* B465:21 (1999)
48. Vasiliev MA, et al (FNAL E866/NuSea Collaboration). *Phys. Rev. Lett.* 83:2304 (1999)
49. Wang XN. *Prog. Theor. Phys. Suppl.* 129:45 (1997)
50. Wang XN. *Phys. Rev. Lett.* 81:2655 (1998); *Phys. Rev.* C58:2321 (1998)
51. Gyulassy M, Lévai P. *Phys. Lett.* B442:1 (1998)
52. Gyulassy M. In *Last Call for RHIC Predictions*, ed. S Bass, et al. *Nucl. Phys.* A661:205c (1999)
53. Gyulassy M, Lévai P, Vitev I. hep-ph/9907343 (1999); hep-ph/9907461 (1999)
54. Lokhtin IP. hep-ph/9904418 (1999)
55. Lokhtin IP, Sarycheva LI, Snigirev AM. hep-ph/9906369 (1999)
56. Wang XN, Huang Z, Sarcevic I. *Phys. Rev. Lett.* 77:231 (1996)
57. Wang XN, Huang Z. *Phys. Rev.* C55:3047 (1997)
58. McGaughey PL, Moss JM, Peng JC. *Annu. Rev. Nucl. Part. Sci.* 49:217 (1999)
59. Shuryak E. *Phys. Rev.* C55:961 (1997)
60. Lin Z, Vogt R, Wang XN. *Phys. Rev.* C57:899 (1998)
61. Lin Z, Vogt R. *Nucl. Phys.* B544:339 (1999)
62. Gallmeister K, Kämpfer B, Pavlenko OP. *Phys. Rev.* C57:3276 (1998); *Prog. Part. Nucl. Phys.* 42:335 (1999)
63. Biro TS, et al. *Phys. Rev.* C48:1275 (1993)

64. Geiger K. *Phys. Rev. D* 56:2665 (1997)
65. Wang XN. *Phys. Rep.* 280:287 (1997)
66. Wong SMH. *Phys. Rev.* C54:2588 (1996); *Phys. Rev.* C56:1075 (1997)
67. Srivastava DK. *Nucl. Phys.* A647:136 (1999)
68. Müller B. nucl-th/9902065 (1999)
69. Eskola KJ. hep-ph/9911350 (1999)
70. Cleymans J, Goloviznin VV, Redlich K. *Quark-Gluon Plasma 2*, ed. RC Hwa, p. 454. Singapore: World Sci. (1995)
71. Harris JW, Müller B. *Annu. Rev. Nucl. Part. Sci.* 46:71 (1996)
72. Sterman G, et al. *Rev. Mod. Phys.* 67:157 (1995)
73. Dokshitzer YL. *Proc. 29th ICHEP*, ed. A Astbury, et al, 1:305. Singapore: World Sci. (1999)

Annual Review of Nuclear and Particle Science
Volume 50, 2000

CONTENTS